

Article

Lead-Free Cs₃Bi₂Br₉ Perovskite Quantum Dots for Detection of Heavy Metal Cu²⁺ Ions in Seawater

Yuefeng Gao ^{1,*} and Baojiu Chen ²

¹ College of Marine Engineering, Dalian Maritime University, Dalian 116026, China

² School of Science, Dalian Maritime University, Dalian 116026, China; bjchen@dmlu.edu.cn

* Correspondence: yue232feng@163.com; Tel.: +86-0411-8472-9314

Abstract: Seawater pollution caused by heavy metal ions is a growing concern among the public. Perovskite quantum dots (PeQDs) are ideal probes for detecting metal ions due to their exceptional sensing characteristics, including remarkable sensitivity, low detection limit, and good selectivity. However, traditional lead-based PeQDs exhibit drawbacks related to lead toxicity and poor water stability. Herein, lead-free halide PeQDs Cs₃Bi₂Br₉ were synthesized using Bi³⁺ instead of Pb²⁺ via the ligand-assisted reprecipitation method. The luminescence performance of the precursor is analyzed with respect to the reaction conditions. The results reveal that the optimal reaction temperature is 80 °C, the ideal octylamine dosage is 35 μL, and the most effective reaction time is 10 min. Photoluminescence spectra of Cs₃Bi₂Br₉ are analyzed at various temperatures and demonstrate that fluorescence intensity decreases as temperature increases. The value of the exciton binding energy (E_b) is determined to be 88.6 meV. Cs₃Bi₂Br₉ PeQDs synthesized under the optimum reaction conditions are utilized as fluorescent probes to detect copper ions in seawater. Results from experiments demonstrate that the presence of copper ions markedly quenched the photoluminescence of Cs₃Bi₂Br₉ owing to the effective transfer of electrons from Cs₃Bi₂Br₉ to Cu²⁺. A strong linear correlation between the degree of quenching and the contents of Cu²⁺ is observed. Cs₃Bi₂Br₉ PeQDs demonstrate a sensitivity and detection limit of 1.21 μM⁻¹ and 98.3 nM, respectively. Furthermore, this probe exhibits good photostability, water stability, and selectivity for copper ions, thereby indicating its potential for detecting marine heavy metal contaminants.



Citation: Gao, Y.; Chen, B. Lead-Free Cs₃Bi₂Br₉ Perovskite Quantum Dots for Detection of Heavy Metal Cu²⁺ Ions in Seawater. *J. Mar. Sci. Eng.* **2023**, *11*, 1001. <https://doi.org/10.3390/jmse11051001>

Academic Editor: Gerardo Gold Bouchot

Received: 11 April 2023

Revised: 29 April 2023

Accepted: 6 May 2023

Published: 8 May 2023



Copyright: © 2023 by the authors. Licensee MDPI, Basel, Switzerland. This article is an open access article distributed under the terms and conditions of the Creative Commons Attribution (CC BY) license (<https://creativecommons.org/licenses/by/4.0/>).

Keywords: lead-free perovskite quantum dots; energy transfer; fluorescence quenching; seawater Cu²⁺ detection

1. Introduction

Industrialization has resulted in the discharge of wastewater containing heavy metals into the ocean through various channels, leading to an elevation in the level of heavy metal ions (such as Cu²⁺, Hg²⁺, Pb²⁺, etc.) in seawater and the degradation of the marine ecological environment. Copper, among these elements, is a necessary trace element for marine organisms, playing a crucial role in their metabolic processes and life activities [1,2]. The concentration of copper in seawater is generally in the range of 0.5–4.5 nM, and in the surface seawater of the open ocean far from land, the concentration of copper is usually less than 1 nM [3]. However, marine organisms are sensitive to copper ions, and even a slight excess concentration can threaten their growth and health [4–6]. The accumulation and dissemination of copper toxins throughout the food chain can result in a risk to human health and the ecosystem [7–9]. Consequently, the development of sensitive and rapid techniques for detecting copper ion concentrations in seawater is of utmost need to safeguard the marine environment and ensure human health.

Traditional methods for detecting copper ions comprise Atomic Absorption Spectroscopy (AAS), Atomic Fluorescence Spectroscopy (AFS), Atomic Emission Spectroscopy

(AES), X-Ray Fluorescence spectrum (XRF), Inductively Coupled Plasma (ICP), and electrochemical methods [10–13]. Although these analytical techniques are accurate and sensitive, they require complex sample preparation procedures, making the detection process demanding and time-consuming. This limitation hinders their application in the marine field, where high efficiency and low cost are essential [14]. To address this issue, simple, fast, economic, and sensitive detection technologies and methods are needed. The utilization of fluorescent probes containing organic dyes and quantum dots (QDs) is a promising approach for detecting Cu^{2+} because of their high sensitivity, selectivity, and specificity [15–17]. As inorganic probes, QDs have remarkable features of component- and size-adjustable photoluminescence and better photobleaching resistance, which fascinates the public [18–20]. In spite of this, some inorganic probes, including CdS, CdSe, and CdTe QDs, have been reported to be toxic, which could potentially jeopardize the environment and human health [21–23]. Thus, developing eco-friendly and non-toxic probes for detecting Cu^{2+} is crucial.

In recent years, inorganic perovskite CsPbX_3 ($X=\text{Cl}$, Br , or I) has been garnering attention as a highly luminescent material owing to its exceptional photoluminescence quantum yield (PLQY), narrow emission peak, and spectral coverage of the entire visible range (380 nm~760 nm) [24–29]. These PeQDs have the potential to serve as excellent materials for detecting Cu^{2+} due to their exceptional optical properties. Previous reports have employed CsPbBr_3 and CsPbI_3 PeQDs as fluorescence probes for Cu^{2+} detection [30–32]. Despite their excellent properties, their instability in water and lead toxicity present significant obstacles to their use in detecting Cu^{2+} in seawater. Consequently, it is essential to develop lead-free PeQDs as an ideal candidate for detecting Cu^{2+} in seawater. To this end, researchers have substituted lead with other elements such as Sn and Ge [33,34]. However, these probes are highly susceptible to oxidation, leading to poor stability and low PLQY [35–38]. Bi has emerged as a promising alternative to Pb in synthesizing lead-free PeQDs, as it is environmentally friendly, non-toxic, and cost-effective [39,40]. Thus, Bi can be considered an excellent alternative to Pb for synthesizing lead-free PeQDs that can be utilized as fluorescent probes for Cu^{2+} detection in seawater.

The objective of this research is to investigate the synthesis and use of $\text{Cs}_3\text{Bi}_2\text{Br}_9$ PeQDs as a potential environmentally friendly and non-toxic probe for detecting Cu^{2+} in seawater. The probe was synthesized via the ligand-assisted reprecipitation approach. In order to optimize the synthesis conditions, control experiments were designed with reaction time, reaction temperature, and dosage of octylamine added into precursor solution as variables. The most favorable parameters were determined to be a reaction temperature of 80 °C, a reaction duration of 10 min, and an octylamine addition dosage of 35 μL , which resulted in the highest emission intensity of $\text{Cs}_3\text{Bi}_2\text{Br}_9$ PeQDs. X-Ray Diffraction (XRD) was employed to examine the phase and structure of $\text{Cs}_3\text{Bi}_2\text{Br}_9$, and the element composition and ratio of the synthesized $\text{Cs}_3\text{Bi}_2\text{Br}_9$ were confirmed by Energy Dispersive Spectrometry (EDS). The luminescence properties of the $\text{Cs}_3\text{Bi}_2\text{Br}_9$ were characterized by measuring the emission, excitation, and absorption spectra. Additionally, the temperature-sensing spectrum of the sample was tested to explore its various characteristics at different temperatures, and the activation energy was calculated. In order to evaluate the practical application of $\text{Cs}_3\text{Bi}_2\text{Br}_9$ PeQDs for detecting copper ions in seawater, the detection range and sensitivity were determined by measuring and analyzing the emission spectra of $\text{Cs}_3\text{Bi}_2\text{Br}_9$ PeQDs after adding different concentrations of copper ions. The selectivity of the $\text{Cs}_3\text{Bi}_2\text{Br}_9$ PeQDs to Cu^{2+} was also verified, and the results showed that solely copper ions could suppress the PL of QDs. However, the introduction of other metal ions, such as Zn^{2+} , Mg^{2+} , Sn^{2+} , Mn^{2+} , Ni^{2+} , Pb^{2+} , and In^{3+} ions, did not yield noticeable alterations in the emission spectra.

Compared with previous studies [30–32], this work replaced the Pb element with the eco-friendly and non-toxic Bi element [38] and synthesized $\text{Cs}_3\text{Bi}_2\text{Br}_9$ as a seawater copper ion detection probe to avoid secondary pollution to the environment during the detection process. In addition, most of the previous lead-based perovskite detection mediums for copper ions were non-polar solvents such as cyclohexane, edible oil, or industrial oil, and

there were few studies on the detection of metal ions in water. The main research medium of this work is seawater solution, which aims to detect marine heavy metal pollutants.

2. Materials and Methods

2.1. Materials

BiBr₃ (≥98%), CsBr (≥99.5%), and InCl₃ (≥99.9%) were purchased from Macklin (<http://www.macklin.cn>, accessed on 16 December 2021). Oleylamine (99%), Dimethyl sulfoxide (DMSO, AR, ≥99%), and oleic acid (OA, AR) were purchased from Aladdin (<https://www.aladdin-e.com>, accessed on 10 July 2021).

Ethanol (CH₃COOH, ≥99.7%), CuCl₂ (≥99%), PbCl₂ (≥99.5%), MgCl₂ (≥98%), NiCl₂ (≥98%), and MnCl₂ (≥99%) were obtained from Damao Chemical Reagent Factory. ZnCl₂ (≥98%) was procured from Sinopharm Chemical Reagent Co., Ltd. (Shanghai, China). SnCl₂ (≥98%) was procured from XILONG SCIENTIFIC (<http://www.xlhg.com>, accessed on 16 December 2021). All purchased chemicals were used as received without further treatment.

2.2. Synthesis of Cs₃Bi₂Br₉

To prepare a clear precursor, a mixture of CsBr (0.043 g), BiBr₃ (0.060 g), DMSO (3 mL), and Oleylamine (35 μL) was stirred for 5 min in a 10 mL vial. In another 10 mL vial, 5 mL ethanol and 0.5 mL OA were thoroughly stirred at 80 °C to ensure full mixing. The precursor solution (0.5 mL) was then rapidly injected into the mixture and vigorously stirred for 10 min to form a colloidal solution. Cs₃Bi₂Br₉ PeQDs were obtained by centrifuging the solution at 9000 rpm for 10 min, and subsequently dissolving the resulting precipitation in ethanol.

2.3. Control Experiment

To investigate the reaction conditions of Cs₃Bi₂Br₉ PeQDs, three sets of control experiments were conducted by varying the dosage of octylamine, reaction time, and reaction temperature, respectively. Four conditions were tested for each control experiment, including the amount of octylamine (10 μL, 20 μL, 35 μL, and 45 μL), reaction time (5 min, 10 min, 15 min, and 20 min), and reaction temperature (25 °C, 50 °C, 80 °C, and 120 °C). The sample preparation process was identical to the synthesis of Cs₃Bi₂Br₉ PeQDs described above, with the same materials and procedures used under different reaction conditions.

2.4. Photostability and Water Stability Experiment

Photostability: The fluorescence spectrum of the unirradiated sample was first examined. Subsequently, a quartz cuvette containing 2 mL of PeQDs solution was exposed to a 405 nm UV lamp emitting 6 W of power, located at a distance of 1 cm. After an irradiation time of 3 h had been reached, the sample was again subjected to fluorescence spectrum measurement. Subsequently, the sample was continuously irradiated, and the corresponding spectra were measured at different cumulative times.

Water stability: Firstly, the fluorescence spectrum of the sample was tested without water. Subsequently, 2 mL of deionized water was added to 2 mL of Cs₃Bi₂Br₉ solution, and the mixture was thoroughly stirred in the air. The fluorescence spectrum of the solution was then measured at different times. The test conditions for the CsPbBr₃ PeQDs remained the same as described above.

2.5. Sensitivity and Selectivity of Cu²⁺ Detection

To assess the detection sensitivity of Cs₃Bi₂Br₉ to Cu²⁺, nine cuvettes were prepared. Each cuvette contained 20 μL of Cs₃Bi₂Br₉, 2 mL of ethanol, and 1 mL of seawater, serving as the detection probe. One solution was used as the blank control sample. Subsequently, 50 μL of prepared copper ions solution was separately added to the other eight solutions, resulting in final concentrations of 0, 150 nM, 300 nM, 450 nM, 600 nM, 750 nM, 900 nM, 1050 nM, and 1200 nM, respectively. The emission spectra were measured by a fluorescence

spectrometer with excitation light at a wavelength of 405 nm, a slit width of 10 nm, and a photomultiplier voltage of 700 V.

In addition, in order to verify the selectivity of $\text{Cs}_3\text{Bi}_2\text{Br}_9$ PeQDs to copper ions, the $\text{Cs}_3\text{Bi}_2\text{Br}_9$ solution was first diluted to 1.0×10^{-4} M at room temperature. Next, a clear Cu^{2+} solution was prepared by dissolving 0.05 mmol of $\text{CuCl}_2 \cdot 2\text{H}_2\text{O}$ into 5 mL purified seawater for detection. A series of solutions containing various concentrations of copper ions were mixed with the $\text{Cs}_3\text{Bi}_2\text{Br}_9$ solution, then the emission spectra and PL decay curves were determined individually.

To verify the selectivity of $\text{Cs}_3\text{Bi}_2\text{Br}_9$ for Cu^{2+} ions, the aforementioned procedure was employed to prepare multiple types of other ions, including Zn^{2+} , Mg^{2+} , Sn^{2+} , Mn^{2+} , Ni^{3+} , Pb^{2+} , and In^{3+} (2 μM). These ions were mixed with $\text{Cs}_3\text{Bi}_2\text{Br}_9$ PeQDs solution, and the changes in fluorescence intensity were measured.

2.6. Characterization

The surface features of the prepared samples were examined using a SUPRA 55 field emission Scanning Electron Microscope (SEM) (ZEISS, Germany), a JEM-2000EX Transmission Electron Microscope (TEM) (JEOL Ltd., Akishima, Japan), and a JEM-2100 High-Resolution Transmission Electron Microscope (HRTEM) (JEOL Ltd., Akishima, Japan) with operating voltages of 5 kV, 120 kV, and 200 kV, respectively. The Energy Dispersive Spectrometer (EDS) spectra were analyzed using an OXFORD X-MaxN SEM (Oxford Instruments, Abingdon, UK). The phase structure of the samples was obtained via X-Ray Diffraction (XRD, D/max-rA power diffractometer (Rigaku, Tokyo, Japan) with Cu-KR radiation, $\lambda = 1.54178 \text{ \AA}$). A UV-3600PC UV-Vis scanning spectrophotometer (Shimadzu, Kyoto, Japan) was used to measure UV/vis absorption spectra. A Hitachi F-4600 fluorescence spectrophotometer was utilized to measure the emission spectrum of the quantum dots with a slit width of 10 nm, voltage of 700 V, excitation wavelength of 405 nm using a Xenon lamp, and wavelength range of 425 nm~600 nm.

3. Results and Discussion

3.1. Effects of Different Conditions on the Fluorescent Properties of $\text{Cs}_3\text{Bi}_2\text{Br}_9$

The ligand-assisted reprecipitation method was utilized to synthesize $\text{Cs}_3\text{Bi}_2\text{Br}_9$ PeQDs. To determine the optimal reaction conditions, control experiments were conducted by varying three factors: reaction time, reaction temperature, and the dosage of octylamine added into the precursor solution. The fluorescence spectra of $\text{Cs}_3\text{Bi}_2\text{Br}_9$ PeQDs synthesized at different temperatures (25 °C, 50 °C, 80 °C, and 120 °C) are shown in Figure 1a. It is evident that the sample exhibited a stronger emission peak at ~480 nm when the reaction temperature was 80 °C. In Figure 1b, the fluorescence spectra of $\text{Cs}_3\text{Bi}_2\text{Br}_9$ PeQDs as reaction time varies (5 min, 10 min, 15 min, and 20 min) are shown. When the reaction duration was 10 min, it was apparent that the sample exhibited a more prominent emission peak. This is because the crystal nucleus of the sample grows with more energy over time, resulting in larger sizes. The crystallinity of the crystal also improves, resulting in increased fluorescence intensity. However, prolonged reaction time can result in decreased fluorescence intensity, possibly caused by the introduction of unpredictable defects during crystal growth [38]. Figure 1c shows the control experiment of changing the dosage of octylamine added. The dosage of octylamine added into the precursor solution was varied between 10 μL , 20 μL , 35 μL , and 45 μL . It is evident that when the dosage of octylamine added is low, the fluorescence intensity increases with the increase in dosage. When the octylamine dosage increases to 35 μL , there is a significant improvement in the fluorescence intensity of the sample, which indicates a significant improvement in the crystal quality of $\text{Cs}_3\text{Bi}_2\text{Br}_9$ PeQDs. Therefore, it can be concluded that the dosage of ligand amine is a crucial factor in controlling crystallization kinetics. However, a minor reduction in fluorescence intensity is noticeable with an increase in the quantity of octylamine. This could be because the amine may form complexes with BiBr_3 , which reduces the yield of $\text{Cs}_3\text{Bi}_2\text{Br}_9$ and hence the luminous intensity. In conclusion, the control experiments indicated that $\text{Cs}_3\text{Bi}_2\text{Br}_9$

exhibited a strong fluorescence intensity when the reaction time was 10 min, the reaction temperature was 80 °C, and the dosage of octylamine was 35 μ L.

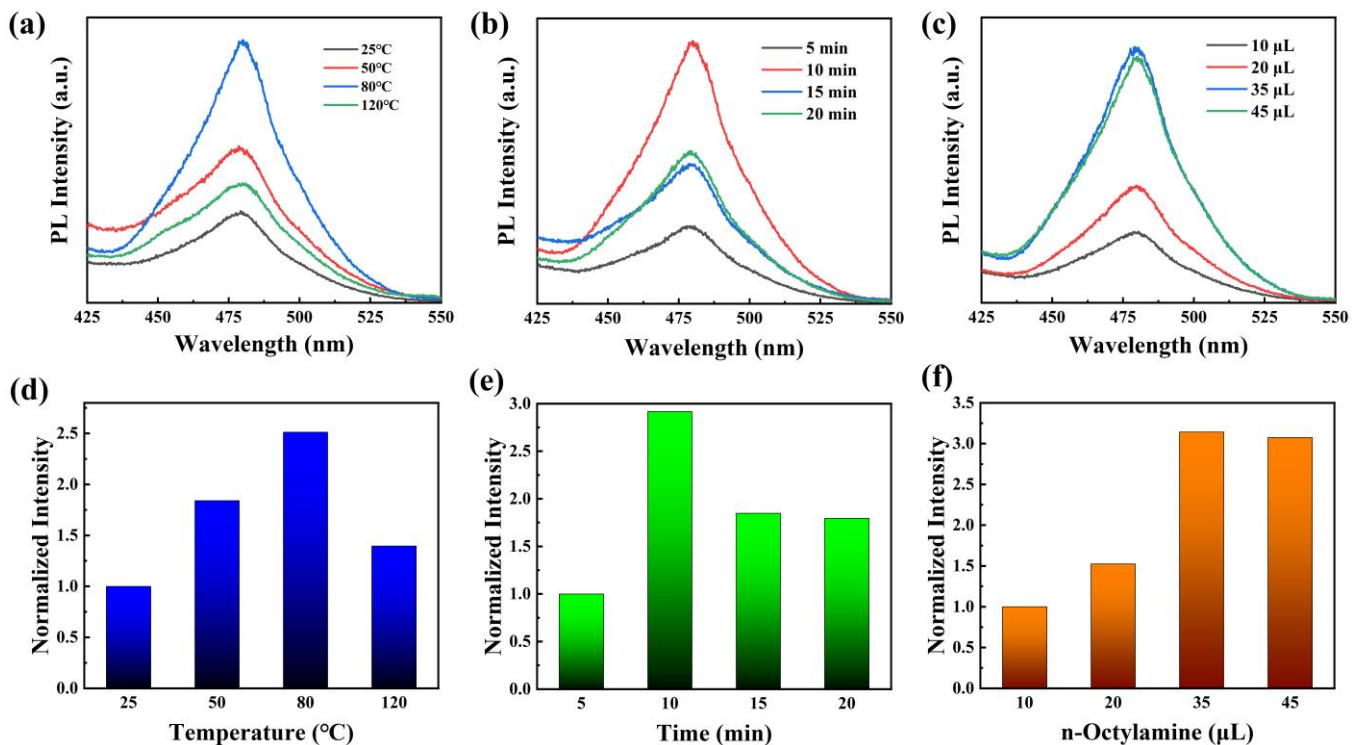


Figure 1. PL spectra of Cs₃Bi₂Br₉ PeQDs with various (a) reaction temperatures, (b) reaction times, and (c) dosages of octylamine. (d–f) Normalized integrated intensity with different reaction conditions.

3.2. Characterization of Cs₃Bi₂Br₉ PeQDs

Based on the optimal conditions obtained from the aforementioned experiments, Cs₃Bi₂Br₉ PeQDs were successfully synthesized, and their morphology was thoroughly characterized. The TEM image in Figure 2a reveals that the PeQDs are spherical with no apparent agglomeration. The inset of Figure 2a is the HR-TEM image of a single quantum dot of Cs₃Bi₂Br₉, which shows clear lattice fringes, indicating that the quantum dot exhibited good crystalline quality. According to the Fourier transform, the lattice spacing can be measured to be 3.3 Å, which corresponds to the (003) crystal plane of Cs₃Bi₂Br₉. The XRD pattern of the QDs (Figure 2b) highly matched with the standard PDF card JCPDS 44-0714, indicating that the PeQDs have a trigonal phase. Furthermore, the sharp tangent diffraction peak indicates that the PeQDs possess high crystallinity. The EDS result (Figure 2c) shows that the molecular ratio of cesium, bismuth, and bromine is about 3.04:2.01:9.26, which is close to the stoichiometric ratio of 3:2:9, further demonstrating the successful preparation of monodisperse Cs₃Bi₂Br₉ PeQDs.

3.3. Optical Properties of Cs₃Bi₂Br₉ PeQDs

Figure 3a displays the absorption and emission spectra of Cs₃Bi₂Br₉ PeQDs. The absorption spectrum is depicted by the dashed line, while the emission spectrum is represented by the solid line. Upon excitation at 405 nm, the PeQDs exhibit an emission peak at 480 nm, with a full width at half maximum (FWHM) of approximately 40.3 nm. The absorption spectrum indicates an absorption peak located at 457 nm. Furthermore, the Stokes shift of the quantum dots is relatively small, calculated to be 23 nm. The excitation spectrum of Cs₃Bi₂Br₉ was determined by observing changes in the emission peak position at 480 nm (Figure 3b), and the peak excitation occurred at 405 nm. Figure 3c shows the excitation-dependent emission behavior of Cs₃Bi₂Br₉ PeQDs, which demonstrates that as the excitation wavelength increases, the position of the emission peak has a certain

red-shift, and the emission intensity is the strongest at the excitation wavelength of 405 nm. To explore the exciton dynamics of Cs₃Bi₂Br₉, the time-resolved fluorescence decay curve was measured, which is exhibited in Figure 3d. The curve was perfectly fitted to determine the average fluorescence decay lifetime using the double e-exponential formula:

$$A(t) = A_1 \exp\left(-\frac{t}{\tau_1}\right) + A_2 \exp\left(-\frac{t}{\tau_2}\right) \quad (1)$$

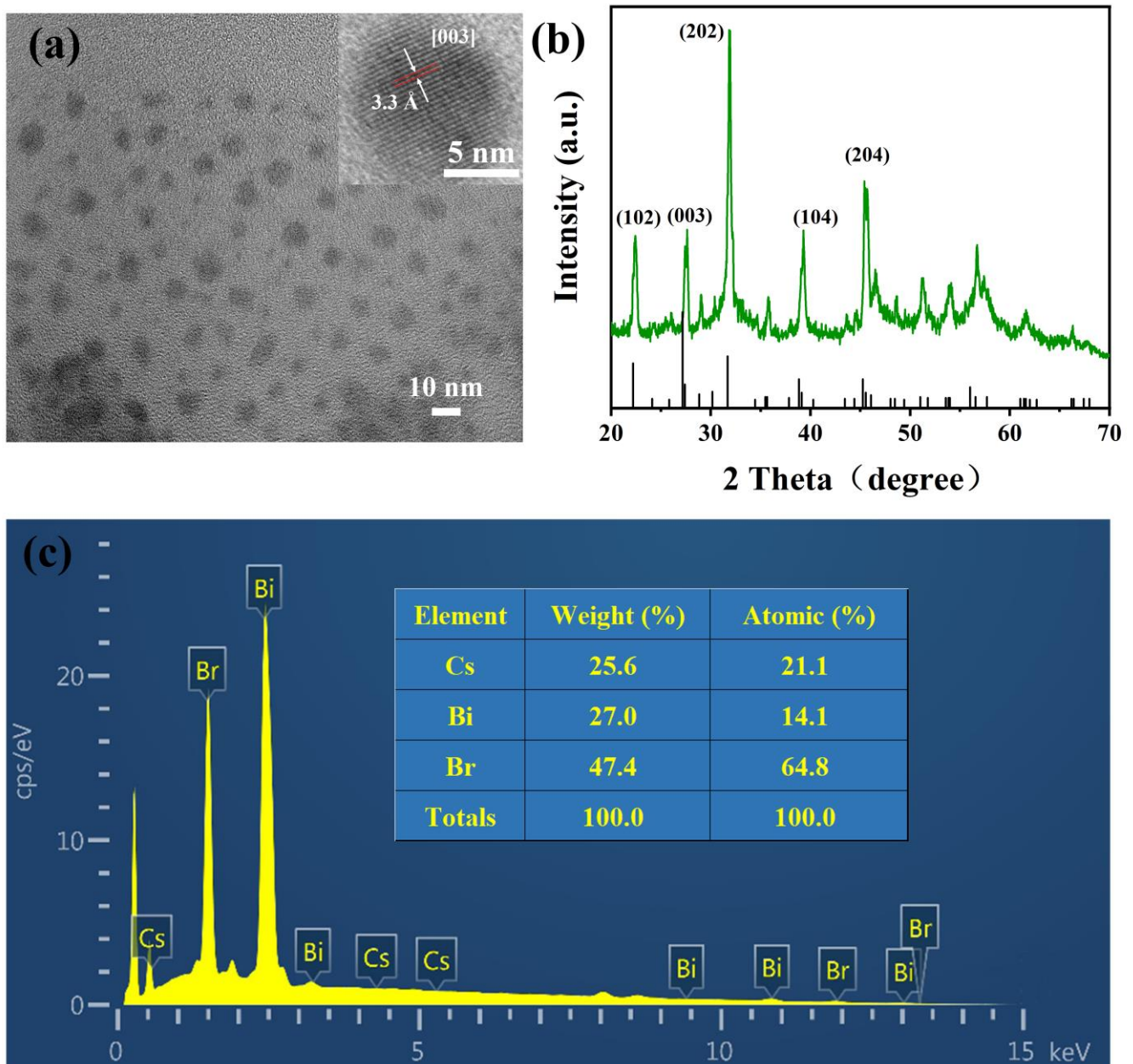


Figure 2. (a) TEM image of Cs₃Bi₂Br₉ PeQDs (Insert: HR-TEM image). (b) XRD patterns of Cs₃Bi₂Br₉ PeQDs. (c) EDS spectrum diagram of Cs₃Bi₂Br₉ PeQDs.

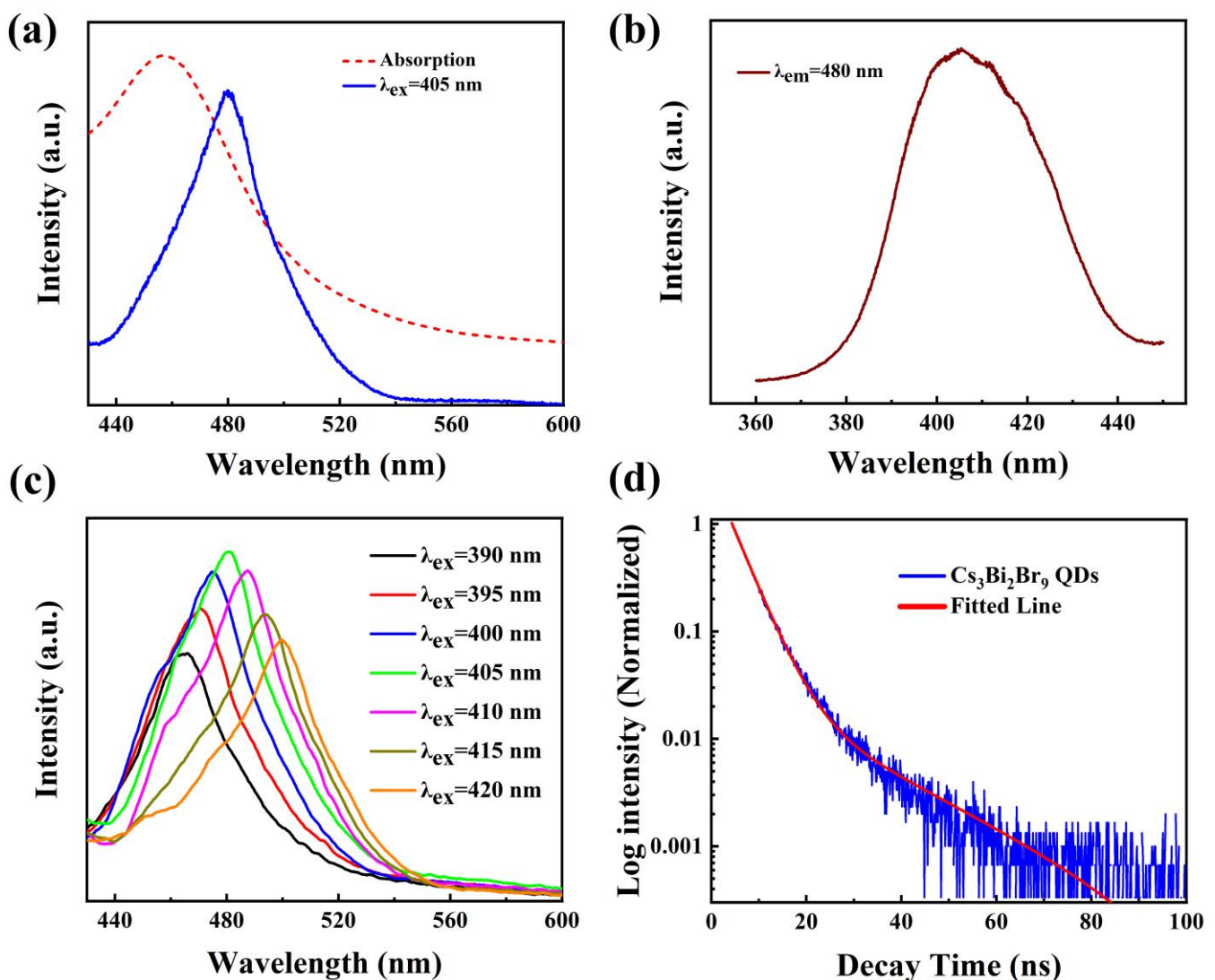


Figure 3. (a) Absorption and emission spectrum (excited by 405 nm). (b) Excitation spectrum (monitored at 480 nm). (c) Excitation-dependent emission behavior. (d) Time-resolved fluorescence spectra.

The fitting curve reveals that the fluorescence decay of quantum dots follows a double exponential form, with the short PL lifetime accounting for 98.8% and a value of 3.98 ns, while the long lifetime accounts for 1.2% and has a value of 19.54 ns. The short lifetime of quantum dots is mainly attributed to direct radiation recombination of excitons after photoexcitation, whereas the long-lived component may be associated with exciton trapping by surface defects of quantum dots [38]. In this study, the short lifetime almost entirely dominates the lifetime, indicating that the luminescence of Cs₃Bi₂Br₉ quantum dots is primarily controlled by exciton radiation recombination.

3.4. Photostability and Water Stability

Figure 4a displays the fluorescence spectra of Cs₃Bi₂Br₉ PeQDs under UV light irradiation at various illumination times. As the irradiation time increases, the PL peak position of the quantum dots gradually shifts towards the red region, while the intensity initially increases and then decreases. When the irradiation time is short, the luminescence of the QDs gradually intensifies. This phenomenon, commonly known as “photoactivation”, is prevalent in QD systems because short-term light can facilitate the elimination of QD surface imperfections and dangling bonds. However, under further ultraviolet light irradi-

ation, the fluorescence of QDs is continuously quenched. A curve showing the relationship between the remaining fluorescence intensity and the irradiation time was obtained by integrating and quantifying the intensity of each fluorescence peak in Figure 4a, as shown in Figure 4b. The fluorescence intensity at a 9 h irradiation time was the highest, being 1.32 times that at the beginning (0 h). After 24 h of irradiation, the remaining PL intensity of the QDs stabilized at about 1.22 times the initial intensity without irradiation. This property is favorable for its application in copper ion sensing.

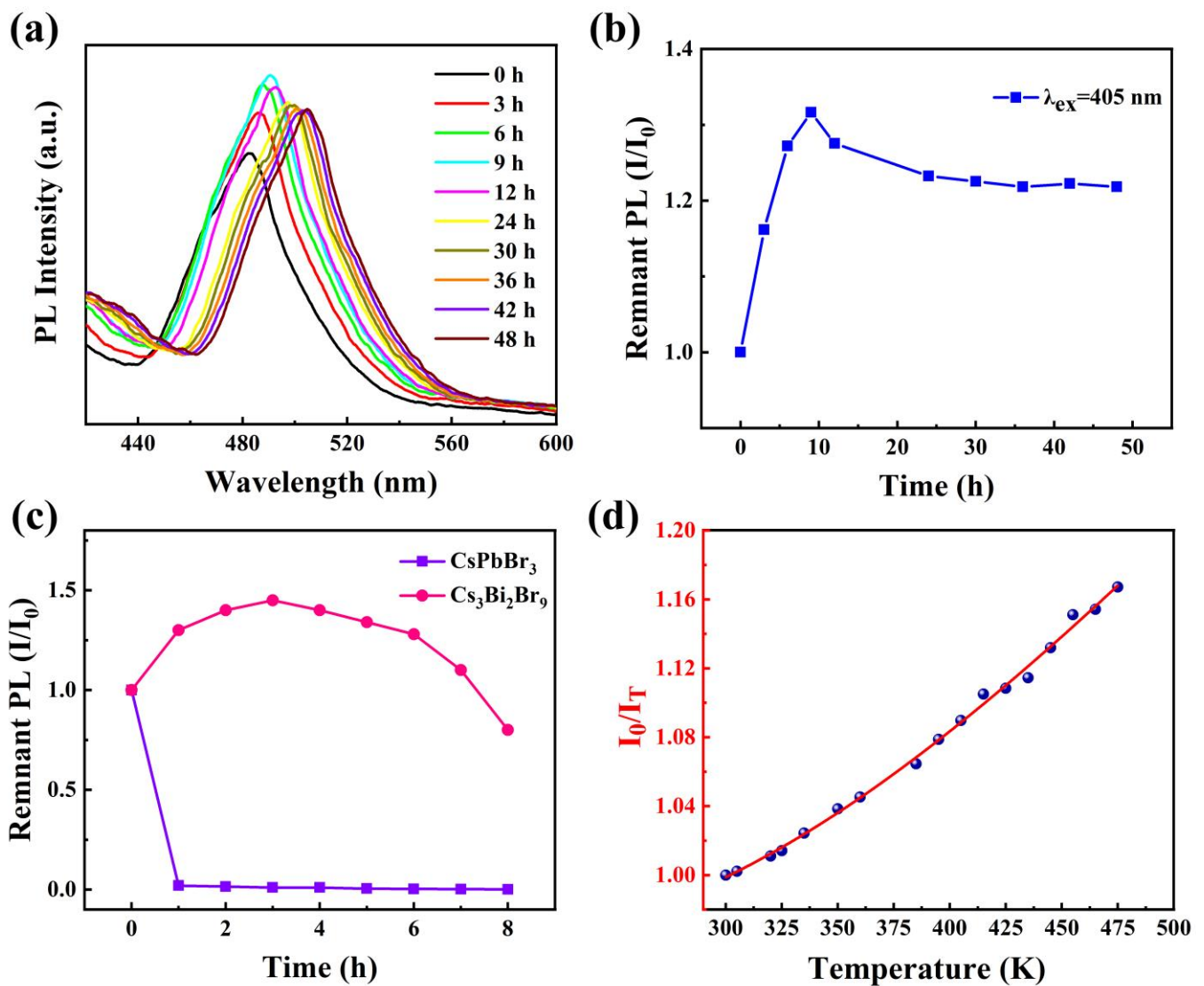


Figure 4. (a) Fluorescence spectra of Cs₃Bi₂Br₉ PeQDs under different UV irradiation times. (b) Curve of remnant fluorescence intensity changing with irradiation time. (c) Remnant PL intensity of Cs₃Bi₂Br₉ and CsPbBr₃ as a function of time in water. (d) Temperature-dependent photoluminescence ratio with the temperature rising.

To assess the water stability of Cs₃Bi₂Br₉ PeQDs, a comparison was made between CsPbBr₃ and Cs₃Bi₂Br₉. Figure 4c illustrates the changes in fluorescence intensity of both types of QDs over time upon the addition of 2 mL of deionized water. The fluorescence of CsPbBr₃ PeQDs was rapidly quenched, while that of Cs₃Bi₂Br₉ PeQDs was observed to increase by nearly 1.4 times. Additionally, after being exposed to air for 8 h, the corresponding fluorescence intensity was reduced by 20%, indicating a certain level of water stability.

3.5. Performance at Different Temperatures

In order to further investigate the photoluminescence decay mechanism of Cs₃Bi₂Br₉, the PL spectra were measured by exciting light of 405 nm at various temperatures from 300 K to 480 K. A plot was created by plotting the integral fluorescence intensity (I) against temperature, using the equation provided [41,42]:

$$\frac{I_0}{I} = C + A \exp\left(-\frac{E_b}{K_B T}\right) \quad (2)$$

The equation used for the plot involves the I_0 (Integral intensity of PeQDs at 300 K), E_b (Exciton binding energy), and K_B (Boltzmann constant). As illustrated by blue data points in Figure 4d, the fluorescence intensity decreases as the temperature rises. This could be attributed to the intensified thermal vibration of the lattice, which leads to more phonons combining with the excited state electrons and thereby increasing the probability of non-radiative recombination, resulting in luminescence quenching. By fitting the data from Figure 3d with an exponential function (red line), the formula $\frac{I_0}{I} = 0.95 + 3.13 \exp\left(-\frac{1274.42}{T}\right)$ was obtained, which has a good deterministic coefficient ($R^2 > 0.99$). Based on the dataset, Cs₃Bi₂Br₉ PeQDs have an E_b of approximately 88.6 meV, which is higher than the E_b of reference (77.9 meV) [38].

3.6. Detection Performance of Cs₃Bi₂Br₉ for Copper Ions

Cs₃Bi₂Br₉ possesses remarkable optical characteristics and is non-toxic, making it a promising candidate for a fluorescent probe for detecting metal ions with high sensitivity. In this study, Cs₃Bi₂Br₉ was utilized to detect the presence of Cu²⁺ in seawater. Figure 5a reveals that as the content of copper ions varies from 0 to 1200 nM, the PL intensity of Cs₃Bi₂Br₉ PeQDs decreases without any shift in the emission peak wavelength. The exciton emission ($\lambda = 480$ nm) quenches rapidly upon the addition of Cu²⁺. The correlation between the quenching of fluorescence and the concentration of Cu²⁺ can be mathematically modeled using the Stern–Volmer equation [43]:

$$\frac{F_0}{F} = A + K[Q] \quad (3)$$

where F_0 denotes the PL intensity of Cs₃Bi₂Br₉ PeQDs in the absence of copper ions, while F refers to the intensity observed in the presence of copper ions. The value of K , known as the Stern–Volmer constant, is indicative of the sensitivity of the detection.

In Figure 5b, the data points were fitted to a linear regression line, and the resulting equation was found to be $F_0/F = 1.13481 + 1.20810[Q]$ with a high linear correlation coefficient ($R^2 > 0.99$). The fitted line equation exhibits a standard deviation of 0.03529 for the intercept and 0.04339 for the slope. This indicates that the quenching sensitivity is 1.21 μM^{-1} . One way to determine the theoretical detection limit is by employing equation $3\sigma/s$, where s represents the slope. The value of σ denotes the standard deviation of the blank signal, which can be determined using the formula [44]:

$$\sigma = \sqrt{\frac{\sum (F_n - \bar{F})^2}{n}} \quad (4)$$

where the PL intensity of the n th measurement is denoted as F_n , while the average fluorescence intensity is represented by \bar{F} . Consequently, the detection limit is calculated to be 98.3 nM using $3\sigma/s$.

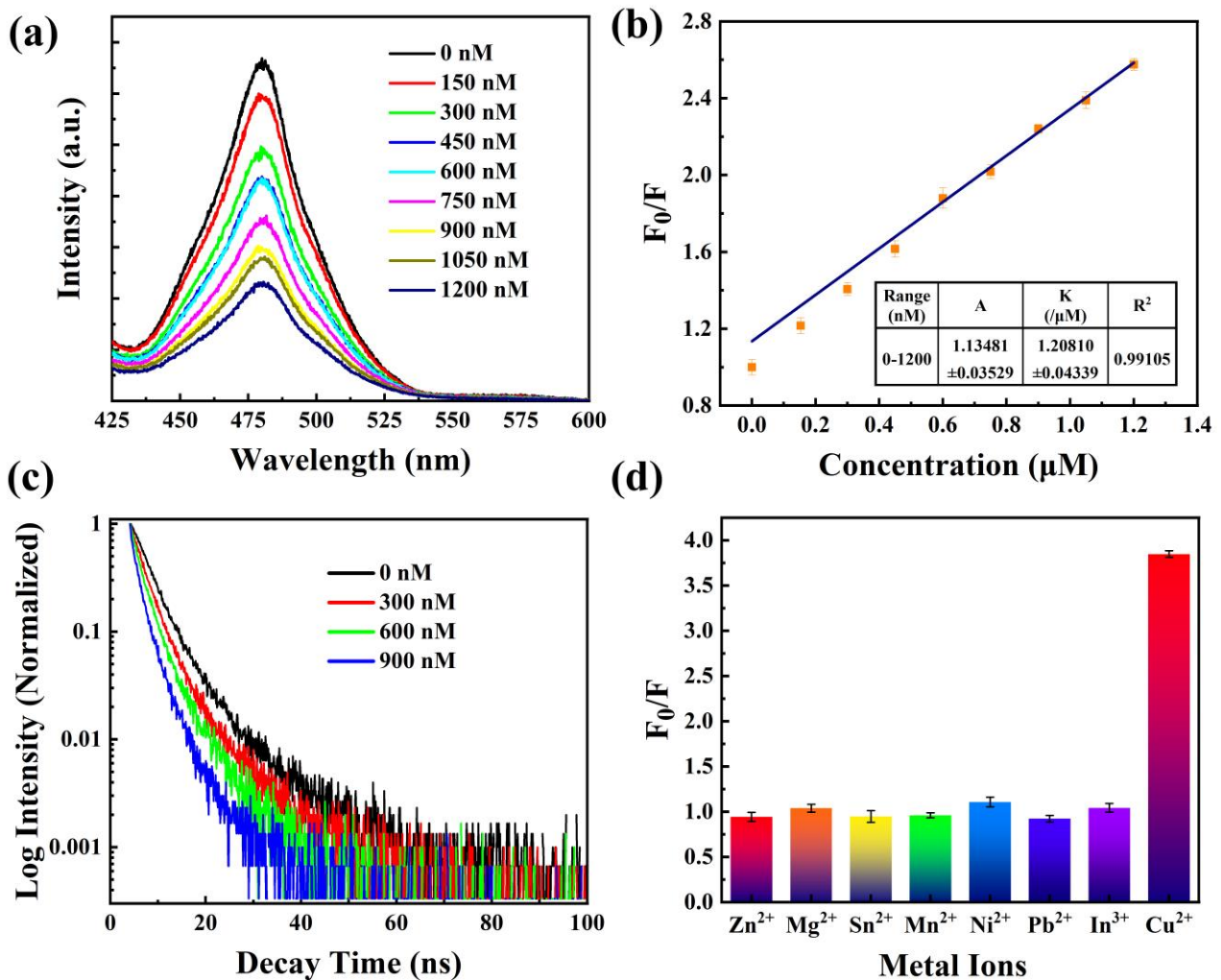


Figure 5. (a) PL intensity of Cs₃Bi₂Br₉ PeQDs at varying Cu²⁺ concentrations. (b) Fitting curve for PL intensity of QDs vs. Cu²⁺ concentration. (c) Time-resolved fluorescence spectra at varying Cu²⁺ concentrations. (d) PL responses of the probe to different metal ions.

Based on the emission spectra analysis, it was found that the shape and position of the peak remain unchanged as the concentration of copper ions increases. This indicates that copper ions only attached to the surface of Cs₃Bi₂Br₉ PeQDs without altering their conformational structure. The valence band maximum (VBM) of Cs₃Bi₂Br₉ PeQDs was primarily influenced by Br, while the Conduct Band Minimum (CBM) was mainly related to Bi [32]. The introduction of Cu²⁺ triggers the emergence of new states at the VBM edge, which predominantly originate from Cu and partially from Br. This results in the formation of Br-Cu-COOH species on the surface of Cs₃Bi₂Br₉. The hole created upon electron formation tends to combine with these new states due to the principle of minimum energy, which could potentially act as an efficient non-radiative recombination pathway for PL quenching. It was observed that other metal ions did not have a significant effect on PL quenching [32]. Therefore, the quenching mechanism of Cs₃Bi₂Br₉ PeQDs is mainly attributed to electron transfer. To further confirm the electron transfer process between Cs₃Bi₂Br₉ PeQDs and Cu²⁺ ions, time-resolved photoluminescence decay curves were obtained at various concentrations of Cu²⁺ in Figure 5c. The fitting results reveal a decrease in the decay lifetime (4.85 ns, 3.45 ns, 2.32 ns, and 0.81 ns) with increasing Cu²⁺ concentration, indicating significant electron transfer from Cs₃Bi₂Br₉ PeQDs to Cu²⁺. The presence of more Cu²⁺ ions results in a faster decay of excitons and a reduction in the decay lifetime.

The selectivity of Cs₃Bi₂Br₉ PeQDs for detecting Cu²⁺ was assessed, and a range of metal ions, such as Zn²⁺, Mg²⁺, Sn²⁺, Mn²⁺, Ni²⁺, Pb²⁺, and In³⁺, were tested at a concentration of 2 μM, concurrently with Cu²⁺. The comparative PL intensity of Cs₃Bi₂Br₉ was measured in the absence and presence of various metal ions. Figure 5d shows that the F₀/F value of Cu²⁺ is 3.85, indicating that the PL intensity decreases significantly after adding Cu²⁺. On the other hand, the F₀/F values of the other metal ions are all around 1, indicating that the PL intensity changes little, and the quenching phenomenon is not distinct. These results demonstrate that Cs₃Bi₂Br₉ PeQDs exhibit high sensitivity and excellent selectivity for detecting Cu²⁺. In order to demonstrate the superiority of the Cs₃Bi₂Br₉ in copper ions sensing performance over other previous probes, different copper ion detection QD probes were compared in Table 1 [30–32,45–49]. It can be seen that although the detection limit of this work is higher than that of other probes, other probes are toxic or contain lead, which can easily cause secondary pollution to the environment. The Cs₃Bi₂Br₉ PeQDs synthesized in this study is a green and environmentally friendly probe. In addition, the detections of copper ions by other perovskites are all in non-polar solvents, such as oil and hexane, while the solvent in this study is the aqueous phase, which is a polar solvent.

Table 1. Cu²⁺ concentration detection by QD-based fluorescence probes.

Probe	Toxicity	Ligand	Sample Solvent	LOD (nM)	Ref.
CdSe	Cadmium-Toxicity	16-mercaptohexadecanoic acid (16-MHA)	aqueous	5	[45]
CdTe nanorods	Cadmium-Toxicity	Thioglycolic acid (TGA)	aqueous	7.8	[46]
CdTe/CdS	Cadmium-Toxicity	3-mercaptopropionic acid (MPA)	aqueous	6.1	[47]
CdTe	Cadmium-Toxicity	Meso-2,3-dimercaptosuccinic acid (DMSA)	aqueous	5.9	[48]
CdTe/CdS	Cadmium-Toxicity	Glyp	aqueous	20	[49]
CsPbBr ₃	Lead-Toxicity	Oleic acid	Oil	2	[32]
CsPbBr ₃	Lead-Toxicity	Oleic acid	Hexane	0.1	[31]
CsPbI ₃ /SiO ₂ IOPCs	Lead-Toxicity	Oleic acid	Oil	0.25/0.34	[30]
Cs ₃ Bi ₂ Br ₉	Eco-Friendly	Oleic acid	aqueous	98.3	This work

3.7. Detection in Real Samples

To assess the practicality of using Cs₃Bi₂Br₉ PeQDs as probes, copper ions in drinking water and seawater were detected. Upon adding copper ion solutions of various concentrations, significant changes in emission spectra were observed. As shown in Table 2, the spectroscopically determined concentrations were found to be very close to the standard concentrations in Tris-HCl buffer, which confirms the usability of Cs₃Bi₂Br₉ PeQDs as a sensing tool for spectrally detecting Cu²⁺ in spiked seawater. In the next step, it is desired to increase the detection sensitivity by increasing the fluorescence intensity of the probe or concentrating the seawater for detection.

Table 2. Cu²⁺ detection in actual samples by Cs₃Bi₂Br₉ probe.

Samples	Added (nM)	Measured (nM)	Recovery (%)
Drinking water	500	493.4	98.7%
	1000	1014.8	101.5%
	2000	2016.5	100.9%
Seawater	500	519.8	104.0%
	1000	1035.4	103.5%
	2000	2047.8	102.4%

4. Conclusions

This study aims to develop a type of PeQDs with lower toxicity than Cs_3PbX_3 PeQDs for detecting copper ions. $\text{Cs}_3\text{Bi}_2\text{Br}_9$ PeQDs were synthesized by replacing Pb^{2+} with Bi^{3+} using a ligand-assisted reprecipitation method at a lower temperature. The method is simple and less toxic, making it suitable for large-scale preparation. The PeQDs exhibit the strongest PL intensity at the reaction temperature of 80 °C, reaction time of 10 min, and the octylamine added dosage of 35 μL . The luminescence of $\text{Cs}_3\text{Bi}_2\text{Br}_9$ is mainly dominated by exciton radiation recombination, with an exciton binding energy of 88.6 meV, indicating high fluorescence intensity. $\text{Cs}_3\text{Bi}_2\text{Br}_9$ PeQDs were utilized as a fluorescent sensor for detecting Cu^{2+} in seawater. The fluorescence of the probe was quenched upon the introduction of copper ions, and the extent of quenching exhibited a linear correlation with the concentration of Cu^{2+} . The sensitivity and detection limit of $\text{Cs}_3\text{Bi}_2\text{Br}_9$ PeQDs were measured to be 1.21 μM^{-1} and 98.3 nM, respectively. The primary cause of quenching is the transfer of electrons from $\text{Cs}_3\text{Bi}_2\text{Br}_9$ to copper ions. Selective experiments revealed that only Cu^{2+} had a discernible effect on the fluorescence of the quantum dots, while other ions did not exhibit any significant impact. This innovative fluorescent probe demonstrates remarkable photostability, water stability, sensitivity, and exceptional selectivity to copper ions, rendering it a highly promising candidate for detecting heavy metal pollutants in marine ecosystems.

Author Contributions: Conceptualization, Y.G.; methodology, Y.G.; software, B.C.; validation, B.C.; formal analysis, Y.G.; investigation, Y.G.; resources, Y.G.; data curation, Y.G.; writing—original draft preparation, Y.G.; writing—review and editing, Y.G. and B.C.; visualization, B.C.; supervision, Y.G.; project administration, Y.G. and B.C.; funding acquisition, Y.G. All authors have read and agreed to the published version of the manuscript.

Funding: This research was funded by the National Natural Science Foundation of China (grant number 52001047 and 52071048), and Fundamental Research Funds for the Central Universities (3132023219, 3132022196, 3132019338).

Institutional Review Board Statement: Not applicable.

Informed Consent Statement: Not applicable.

Data Availability Statement: Not applicable.

Conflicts of Interest: The authors declare no conflict of interest.

References

1. Biswas, H.; Bandyopadhyay, D.; Waite, A. Copper Addition Helps Alleviate Iron Stress in a Coastal Diatom: Response of *Chaetoceros Gracilis* from the Bay of Bengal to Experimental Cu and Fe Addition. *Mar. Chem.* **2013**, *157*, 224–232. [[CrossRef](#)]
2. Jacquot, J.E.; Kondo, Y.; Knapp, A.N.; Moffett, J.W. The Speciation of Copper across Active Gradients in Nitrogen-Cycle Processes in the Eastern Tropical South Pacific. *Limnol. Oceanogr.* **2013**, *58*, 1387–1394. [[CrossRef](#)]
3. Bruland, K.W.; Lohan, M.C. Controls of Trace Metals in Seawater. *Ocean. Mar. Geochem.* **2006**, *6*, 23–47.
4. Huang, W.; Zhou, Y.; Zhao, T.; Tan, L.; Wang, J. The Effects of Copper Ions and Copper Nanomaterials on the Output of Amino Acids from Marine Microalgae. *Environ. Sci. Pollut. Res.* **2022**, *29*, 9780–9791. [[CrossRef](#)]
5. Mandich, M. Ranked Effects of Heavy Metals on Marine Bivalves in Laboratory Mesocosms: A Meta-Analysis. *Mar. Pollut. Bull.* **2018**, *131*, 773–781. [[CrossRef](#)]
6. Malhotra, N.; Ger, T.-R.; Uapipatanakul, B.; Huang, J.-C.; Chen, K.H.-C.; Hsiao, C.-D. Review of Copper and Copper Nanoparticle Toxicity in Fish. *Nanomaterials* **2020**, *10*, 1126. [[CrossRef](#)]
7. Kozłowski, H.; Luczkowski, M.; Remelli, M.; Valensin, D. Copper, Zinc and Iron in Neurodegenerative Diseases (Alzheimer's, Parkinson's and Prion Diseases). *Coord. Chem. Rev.* **2012**, *256*, 2129–2141. [[CrossRef](#)]
8. Brewer, G.J.; Kanzer, S.H.; Zimmerman, E.A.; Celmins, D.F.; Heckman, S.M.; Dick, R. Copper and Ceruloplasmin Abnormalities in Alzheimer's Disease. *Am. J. Alzheimers Dis. Other Dement.* **2010**, *25*, 490–497. [[CrossRef](#)]
9. Hu, H.; Jin, Q.; Kavan, P. A Study of Heavy Metal Pollution in China: Current Status, Pollution-Control Policies and Countermeasures. *Sustainability* **2014**, *6*, 5820–5838. [[CrossRef](#)]
10. Song, Y.; Ma, Q.; Cheng, H.; Liu, J.; Wang, Y. Simultaneous Enrichment of Inorganic and Organic Species of Lead and Mercury in Pg L-1 Levels by Solid Phase Extraction Online Combined with High Performance Liquid Chromatography and Inductively Coupled Plasma Mass Spectrometry. *Anal. Chim. Acta* **2021**, *1157*, 338388. [[CrossRef](#)]

11. Bacon, J.R.; Butler, O.T.; Cairns, W.R.L.; Cook, J.M.; Mertz-Kraus, R.; Tyson, J.F. Atomic Spectrometry Update—A Review of Advances in Environmental Analysis. *J. Anal. At. Spectrom.* **2019**, *34*, 9–58. [[CrossRef](#)]
12. Nguyen, T.T.K.; Luu, H.T.; Vu, L.D.; Ta, T.T.; Le, G.T.H. Determination of Total Mercury in Solid Samples by Anodic Stripping Voltammetry. *J. Chem.* **2021**, *2021*, 8888879. [[CrossRef](#)]
13. Alharthi, S.S.; Fallatah, A.M.; Al-Saidi, H.M. Design and Characterization of Electrochemical Sensor for the Determination of Mercury(II) Ion in Real Samples Based upon a New Schiff Base Derivative as an Ionophore. *Sensors* **2021**, *21*, 3020. [[CrossRef](#)]
14. Lim, J.W.; Kim, T.-Y.; Woo, M.-A. Trends in Sensor Development toward Next-Generation Point-of-Care Testing for Mercury. *Biosens. Bioelectron.* **2021**, *183*, 113228. [[CrossRef](#)] [[PubMed](#)]
15. Mattio, E.; Robert-Peillard, F.; Vassalo, L.; Branger, C.; Margailan, A.; Brach-Papa, C.; Knoery, J.; Boudenne, J.-L.; Coulomb, B. 3D-Printed Lab-on-Valve for Fluorescent Determination of Cadmium and Lead in Water. *Talanta* **2018**, *183*, 201–208. [[CrossRef](#)] [[PubMed](#)]
16. Shi, J.-J.; Zhu, J.-C.; Zhao, M.; Wang, Y.; Yang, P.; He, J. Ultrasensitive Photoelectrochemical Aptasensor for Lead Ion Detection Based on Sensitization Effect of CdTe QDs on MoS₂-CdS:Mn Nanocomposites by the Formation of G-Quadruplex Structure. *Talanta* **2018**, *183*, 237–244. [[CrossRef](#)] [[PubMed](#)]
17. Dumbare, S.; Doshi, A.; Ravindran, S. Rhodamine B and Rhodamine 6G Based Sensing of Copper Ions in Environmental and Biological Samples: Recent Progress. *Pol. J. Environ. Stud.* **2021**, *30*, 3445–3455. [[CrossRef](#)]
18. Zhang, L.; Shang, L.; Dong, S. Sensitive and Selective Determination of Cu²⁺ by Electrochemiluminescence of CdTe Quantum Dots. *Electrochem. Commun.* **2008**, *10*, 1452–1454. [[CrossRef](#)]
19. Rana, M.; Devlal, K. Thioglycolic Acid Capped CdTe Quantum Dots as Sensors for the Detection of Hazardous Heavy Metal Ion Cu²⁺ in Water. *MAPAN-J. Metrol. Soc. India* **2022**, *37*, 41–46. [[CrossRef](#)]
20. Wang, L.; Liu, Z.; Han, J.; Li, R.; Huang, M. Stepwise Synthesis of Au@CdS-CdS Nanoflowers and Their Enhanced Photocatalytic Properties. *Nanoscale Res. Lett.* **2019**, *14*, 148. [[CrossRef](#)]
21. Cui, S.; Xu, S.; Song, H.; Xu, W.; Chen, X.; Zhou, D.; Yin, Z.; Han, W. Highly Sensitive and Selective Detection of Mercury Ions Based on Up-Conversion FRET from NaYF₄:Yb³⁺/Er³⁺ Nanophosphors to CdTe Quantum Dots. *RSC Adv.* **2015**, *5*, 99099–99106. [[CrossRef](#)]
22. Nisha, K.D.; Navaneethan, M.; Dhanalakshmi, B.; Murali, K.S.; Hayakawa, Y.; Ponnusamy, S.; Muthamizhchelvan, C.; Gunasekaran, P. Effect of Organic-Ligands on the Toxicity Profiles of CdS Nanoparticles and Functional Properties. *Colloid Surf. B-Biointerfaces* **2015**, *126*, 407–413. [[CrossRef](#)] [[PubMed](#)]
23. Paithankar, J.G.; Kushalan, S.; Nijil, S.; Hegde, S.; Kini, S.; Sharma, A. Systematic Toxicity Assessment of CdTe Quantum Dots in *Drosophila Melanogaster*. *Chemosphere* **2022**, *295*, 133836. [[CrossRef](#)] [[PubMed](#)]
24. Protesescu, L.; Yakunin, S.; Bodnarchuk, M.I.; Krieg, F.; Caputo, R.; Hendon, C.H.; Yang, R.X.; Walsh, A.; Kovalenko, M.V. Nanocrystals of Cesium Lead Halide Perovskites (CsPbX₃, X = Cl, Br, and I): Novel Optoelectronic Materials Showing Bright Emission with Wide Color Gamut. *Nano Lett.* **2015**, *15*, 3692–3696. [[CrossRef](#)]
25. Liu, B.; Wang, G.; Lu, Y.; Wang, W.; Liu, Z.; Li, J. Zinc Borosilicate Glass-Stabilized CsPbX₃ (X = Cl, Br, I) Perovskite Quantum Dots for Photoluminescence Lighting and Display Applications. *ACS Appl. Nano Mater.* **2022**, *5*, 9503–9513. [[CrossRef](#)]
26. Wang, C.; Zhang, C.; Wang, F.; Chen, J.; Kong, J.; Li, L.; Xu, J.; Zhang, Y. Flexible Cesium Lead Halide CsPbX₃@SiO₂ (X = Cl, Br, I and Their Mixtures) Perovskite Nanocrystal Films. *J. Alloy. Compd.* **2022**, *925*, 166551. [[CrossRef](#)]
27. Li, M.; Zeng, Y.; Qu, X.; Jalalah, M.; Alsareii, S.A.; Li, C.; Harraz, F.A.; Li, G. Biocatalytic CsPbX₃ Perovskite Nanocrystals: A Self-Reporting Nanoprobe for Metabolism Analysis. *Small* **2021**, *17*, 2103255. [[CrossRef](#)]
28. Zhong, Q.; Liu, J.; Chen, S.; Li, P.; Chen, J.; Guan, W.; Qiu, Y.; Xu, Y.; Cao, M.; Zhang, Q. Highly Stable CsPbX₃/PbSO₄ Core/Shell Nanocrystals Synthesized by a Simple Post-Treatment Strategy. *Adv. Opt. Mater.* **2021**, *9*, 2001763. [[CrossRef](#)]
29. Shang, Y.; Li, G.; Liu, W.; Ning, Z. Quasi-2D Inorganic CsPbBr₃ Perovskite for Efficient and Stable Light-Emitting Diodes. *Adv. Funct. Mater.* **2018**, *28*, 1801193. [[CrossRef](#)]
30. Gao, Y.; Xu, S.; Liu, Z.; Yu, K.; Wang, C.; Wu, S.; Wang, J.; Pan, X. Fluorescence Enhanced Microfluidic Sensor with CsPbI₃ Probe for Lubricant Copper Ions On-Site Rapid Detection Based on SiO₂ Inverse Opal Photonic Crystals. *J. Lumin.* **2021**, *238*, 118276. [[CrossRef](#)]
31. Liu, Y.; Tang, X.; Zhu, T.; Deng, M.; Ikechukwu, I.P.; Huang, W.; Yin, G.; Bai, Y.; Qu, D.; Huang, X.; et al. All-Inorganic CsPbBr₃ Perovskite Quantum Dots as a Photoluminescent Probe for Ultrasensitive Cu²⁺ Detection. *J. Mater. Chem. C* **2018**, *6*, 4793–4799. [[CrossRef](#)]
32. Sheng, X.; Liu, Y.; Wang, Y.; Li, Y.; Wang, X.; Wang, X.; Dai, Z.; Bao, J.; Xu, X. Cesium Lead Halide Perovskite Quantum Dots as a Photoluminescence Probe for Metal Ions. *Adv. Mater.* **2017**, *29*, 1700150. [[CrossRef](#)] [[PubMed](#)]
33. Mahesh, K.P.O.; Chang, C.-Y.; Hong, W.-L.; Wen, T.-H.; Lo, P.-H.; Chiu, H.-Z.; Hsu, C.-L.; Horng, S.-F.; Chao, Y.-C. Lead-Free Cesium Tin Halide Nanocrystals for Light-Emitting Diodes and Color down Conversion. *RSC Adv.* **2020**, *10*, 37161–37167. [[CrossRef](#)] [[PubMed](#)]
34. Wu, X.; Song, W.; Li, Q.; Zhao, X.; He, D.; Quan, Z. Synthesis of Lead-Free CsGeI₃ Perovskite Colloidal Nanocrystals and Electron Beam-Induced Transformations. *Chem.-Asian J.* **2018**, *13*, 1654–1659. [[CrossRef](#)]
35. Dolzhenkov, D.S.; Wang, C.; Xu, Y.; Kanatzidis, M.G.; Weiss, E.A. Ligand-Free, Quantum-Confined Cs₂SnI₆ Perovskite Nanocrystals. *Chem. Mat.* **2017**, *29*, 7901–7907. [[CrossRef](#)]

36. Tan, Z.; Li, J.; Zhang, C.; Li, Z.; Hu, Q.; Xiao, Z.; Kamiya, T.; Hosono, H.; Niu, G.; Lifshitz, E.; et al. Highly Efficient Blue-Emitting Bi-Doped Cs₂SnCl₆ Perovskite Variant: Photoluminescence Induced by Impurity Doping. *Adv. Funct. Mater.* **2018**, *28*, 1801131. [[CrossRef](#)]
37. Song, T.-B.; Yokoyama, T.; Aramaki, S.; Kanatzidis, M.G. Performance Enhancement of Lead-Free Tin Based Perovskite Solar Cells with Reducing Atmosphere-Assisted Dispersible Additive. *ACS Energy Lett.* **2017**, *2*, 897–903. [[CrossRef](#)]
38. Leng, M.; Yang, Y.; Zeng, K.; Chen, Z.; Tan, Z.; Li, S.; Li, J.; Xu, B.; Li, D.; Hautzinger, M.P.; et al. All-Inorganic Bismuth-Based Perovskite Quantum Dots with Bright Blue Photoluminescence and Excellent Stability. *Adv. Funct. Mater.* **2018**, *28*, 1704446. [[CrossRef](#)]
39. Wu, D.; Zhao, X.; Huang, Y.; Lai, J.; Li, H.; Yang, J.; Tian, C.; He, P.; Huang, Q.; Tang, X. Lead-Free Perovskite Cs₂AgBiX₆ Nanocrystals with a Band Gap Funnel Structure for Photocatalytic CO₂ Reduction under Visible Light. *Chem. Mat.* **2021**, *33*, 4971–4976. [[CrossRef](#)]
40. Connor, B.A.; Leppert, L.; Smith, M.D.; Neaton, J.B.; Karunadasa, H.I. Layered Halide Double Perovskites: Dimensional Reduction of Cs₂AgBiBr₆. *J. Am. Chem. Soc.* **2018**, *140*, 5235–5240. [[CrossRef](#)]
41. Fang, H.-H.; Wang, F.; Adjokatse, S.; Zhao, N.; Even, J.; Loi, M.A. Photoexcitation Dynamics in Solution-Processed Formamidinium Lead Iodide Perovskite Thin Films for Solar Cell Applications. *Light-Sci. Appl.* **2016**, *5*, e16056. [[CrossRef](#)] [[PubMed](#)]
42. Wright, A.D.; Verdi, C.; Milot, R.L.; Eperon, G.E.; Perez-Osorio, M.A.; Snaith, H.J.; Giustino, F.; Johnston, M.B.; Herz, L.M. Electron-Phonon Coupling in Hybrid Lead Halide Perovskites. *Nat. Commun.* **2016**, *7*, 11755. [[CrossRef](#)]
43. Lu, L.; Tan, T.; Tian, X.; Li, Y.; Deng, P. Visual and Sensitive Fluorescent Sensing for Ultratrace Mercury Ions by Perovskite Quantum Dots. *Anal. Chim. Acta* **2017**, *986*, 109–114. [[CrossRef](#)] [[PubMed](#)]
44. Gao, Y.; Pan, X.; Xu, S.; Liu, Z.; Wang, J.; Yu, K.; Wang, C.; Yuan, H.; Wu, S. Fluorescence-Enhanced Microfluidic Sensor for Highly Sensitive in-Situ Detection of Copper Ions in Lubricating Oil. *Mater. Des.* **2020**, *191*, 108693. [[CrossRef](#)]
45. Chan, Y.; Chen, J.; Liu, Q.; Wark, S.E.; Son, D.H.; Batteas, J.D. Ultrasensitive Copper(II) Detection Using Plasmon-Enhanced and Photo-Brightened Luminescence of CdSe Quantum Dots. *Anal. Chem.* **2010**, *82*, 3671–3678. [[CrossRef](#)] [[PubMed](#)]
46. Liu, M.; Zhao, H.; Quan, X.; Chen, S.; Yu, H. Signal Amplification via Cation Exchange Reaction: An Example in the Ratiometric Fluorescence Probe for Ultrasensitive and Selective Sensing of Cu(II). *Chem. Commun.* **2010**, *46*, 1144–1146. [[CrossRef](#)] [[PubMed](#)]
47. Mei, Y.; Wang, H.; Li, Y.; Pan, Z.; Jia, W. Electrochemiluminescence of CdTe/CdS Quantum Dots with Tripropylamine as Coreactant in Aqueous Solution at a Lower Potential and Its Application for Highly Sensitive and Selective Detection of Cu²⁺. *Electroanalysis* **2010**, *22*, 155–160. [[CrossRef](#)]
48. Wang, P.; Ma, X.; Su, M.; Hao, Q.; Lei, J.; Ju, H. Cathode Photoelectrochemical Sensing of Copper(II) Based on Analyte-Induced Formation of Exciton Trapping. *Chem. Commun.* **2012**, *48*, 10216–10218. [[CrossRef](#)]
49. Liu, S.; Wang, Y.; Han, J. Fluorescent Chemosensors for Copper(II) Ion: Structure, Mechanism and Application. *J. Photochem. Photobiol. C-Photochem. Rev.* **2017**, *32*, 78–103. [[CrossRef](#)]

Disclaimer/Publisher's Note: The statements, opinions and data contained in all publications are solely those of the individual author(s) and contributor(s) and not of MDPI and/or the editor(s). MDPI and/or the editor(s) disclaim responsibility for any injury to people or property resulting from any ideas, methods, instructions or products referred to in the content.